Near infrared photoimmunotherapy in a transgenic mouse model of spontaneous epidermal growth factor receptor (EGFR)-expressing lung cancer

Yuko Nakamura[†], **Zoe Weaver Ohler**[‡], **Deborah Householder**[‡], **Tadanobu Nagaya**[†], **Kazuhide Sato**[†], **Shuhei Okuyama**[†], **Fusa Ogata**[†], **Dagane Daar**[†], **Tieu Hoa**[†], **Peter L. Choyke**[†], and **Hisataka Kobayashi**[*,†]

[†]Molecular Imaging Program, Center for Cancer Research, National Cancer Institute

[‡]Center for Advanced Preclinical Research, Leidos Biomedical Research Inc., Frederick National Laboratory for Cancer Research

Abstract

Near infrared photoimmunotherapy (NIR-PIT) is a new cancer treatment that combines the specificity of antibodies for targeting tumors with the toxicity induced by a sensitive photoabsorber following exposure to NIR light. Most studies of NIR-PIT have been performed in xenograft models of cancer. The purpose of this study was to evaluate the therapeutic effects of NIR-PIT in a transgenic model of spontaneous lung cancer expressing human epidermal growth factor receptor (hEGFR). Mice were separated into 3 groups for the following treatments: (1) no treatment (control); (2) 150 μg of photoabsorber, IR700, conjugated to panitumumab, an antibody targeting EGFR (antibody-photoabsorber conjugate (APC)) i.v. only; (3) 150 μg of APC i.v. with NIR light administration. Each treatment was performed every week up to three weeks. MRI was performed 1 day before and 3, 6, 13, 20, 27, and 34 days after first NIR-PIT. The relative volume of lung tumors was calculated from the tumor volume at each MRI time point divided by the initial volume. Steel's test for multiple comparison was used to compare the tumor volume ratio with that of control. Tumor volume ratio was inhibited significantly in the NIR-PIT group compared with control group (p < 0.01 at all time points). In conclusion, NIR-PIT effectively treated a spontaneous lung cancer in a hEGFR TL transgenic mouse model. MRI successfully monitored the therapeutic effects of NIR-PIT.

Keywords

near infrared photoimmunotherapy; transgenic mouse; lung cancer; MRI

---

[*]Corresponding author: Hisataka Kobayashi, Molecular Imaging Program, Center for Cancer Research, National Cancer Institute, NIH, Building 10, RoomB3B69, MSC1088, Bethesda, MD 20892-1088. Phone: 301-435-4086, Fax: 301-402-3191. kobayash@mail.nih.gov.

Note: none.

INTRODUCTION

Near infrared photoimmunotherapy (NIR-PIT) is a newly developed cancer treatment that employs a targeted monoclonal antibody conjugated to a photoabsorber, IRDye700DX (IR700, silica-phthalocyanine dye; Supplementary figure S1) (1). The first-in-human phase 1 trial of NIR-PIT in patients with inoperable head and neck cancer targeting epidermal growth factor receptor (EGFR) was approved by the US FDA, started in June 2015 (https:// clinicaltrials.gov/ct2/show/NCT02422979), and finished in August 2016. In this trial, patients were injected with an antibody-photoabsorber (IR700) conjugate (APC), RM1929, that binds to target EGFR molecules on the cell membrane of the tumor. About 24 hours later the tumor was exposed to NIR light at a wavelength of 690 nm which is absorbed by IR700. NIR-PIT induces nearly immediate necrotic cell death rather than the apoptotic cell death that is most commonly induced by other cancer therapies.

NIR-PIT has been shown to be effective using a variety of different APCs, each targeting separate overexpressed cell surface receptors in subcutaneously xenografted human tumors (1–6) and lung or peritoneal metastasis (7–10) in athymic mice. However, the xenograft tumor model does not fully represent human cancers as the tumor tends to be monoclonal and there is no immune component to the response. However, such studies are straightforward, easier to perform and at least are suggestive of clinical efficacy. The literature is replete with discrepancies between the aggressive behavior of tumors in patients compared to the relatively mild tumor behavior in the subcutaneously transplanted xenografts in nude mice which tend to grow locally but not to become invasive or metastasize (11,12). The vast majority of human solid tumors, growing subcutaneously in the nude mice, do not metastasize. The subcutaneously transplanted tumors tend to demonstrate local expansive tumor growth with circumscribed tumor borders without apparent invasion (12). This is also true of patient-derived xenograft models (11,13).

Genetically engineered mouse (GEM) models of cancer reproduce the tumor microenvironment, including the intact immune response, more accurately than human cell line xenograft models. Although we have extensively tested NIR-PIT in xenograft models we have not yet done so in transgenic autochthonous models. Evaluation on NIR-PIT in transgenic models of lung adenocarcinoma is somewhat more complex than the xenograft model. The therapeutic effect of cancer treatments can be evaluated by various methods in mice, such as measurement of tumor size measured with a caliper and evaluation of luciferase activity (1,7,14–16). However, measurement of tumor size with a caliper is available only for subcutaneous tumors, while bioluminescence requires the expression of luciferase exclusively in the tumor cells, requiring breeding of additional alleles into GEM models for lung cancer. On the other hand, magnetic resonance imaging (MRI) is a widely used imaging modality that demonstrates both anatomic and functional information in a short time. MRI can repeatedly evaluate any part of the body regardless of the depth and does not need luciferase expression or radiation exposure.

The purpose of this study was to determine the therapeutic effect of NIR-PIT in a human EGFR (hEGFR-TL)-expressing transgenic mouse model for lung adenocarcinoma using MRI. This model expresses human EGFR containing both the L858R and T790M mutations

found in patients, the latter rendering the tumors resistant to EGFR tyrosine kinase inhibitors (TKI). Currently there are few treatment options available for patients with acquired resistance to EGFR TKIs, so evaluation of novel therapeutic strategies is crucial. Existing models for mutant EGFR-induced lung adenocarcinoma in mice generate diffuse tumors that would be more difficult to evaluate by NIR-PIT. Therefore we re-engineered the model to form more nodular, discrete tumors amenable to assessing the value of NIR-PIT in lung cancer.

MATERIALS AND METHODS

Reagents

Water soluble, silica-phthalocyanine derivative, IRDye700DX NHS ester was obtained from LI-COR Bioscience (Lincoln, NE, USA). Panitumumab, a fully humanized IgG2 monoclonal antibodies (mAb) directed against EGFR, was purchased from Amgen (Thousand Oaks, CA, USA). All other chemicals were of reagent grade.

Synthesis of IR700-conjugated panitumumab

Conjugation of dyes with mAb was performed according to previous reports (1,17,18). In brief, panitumumab (1 mg, 6.8 nmol) was incubated with IR700 NHS ester (60.2 μg, 30.8 nmol) in 0.1 mol/L Na_2HPO_4 (pH 8.6) at room temperature for 1 hour. The mixture was purified with a Sephadex G25 column (PD-10; GE Healthcare). The protein concentration was determined with Coomasie Plus protein assay kit (Thermo Fisher Scientific Inc) by measuring the absorption at 595 nm with spectroscopy (8453 Value System; Agilent Technologies). The concentration of IR700 was measured by absorption at 689 nm with spectroscopy to confirm the number of fluorophore molecules conjugated to each mAb. The synthesis was controlled so that an average of three IR700 molecules were bound to a single antibody. We abbreviate IR700 conjugated to panitumumab as pan-IR700.

Generation of transgenic mice

To generate the hEGFR TL transgenic mice, we purchased the human EGFR cDNA with an L858R mutation from Addgene (www.addgene.org; plasmid #11012) and cloned it into the pTRE-tight vector (Clontech, Mountain View, CA). Site-directed mutagenesis was performed to produce the T790M mutation. The construct was then digested to release the entire allele containing TRE-EGFR-L858R-T790M-SV40 polyA. Transgenic mice were then generated by injection of the construct into FVB/N fertilized mouse eggs. EGFR-L858R-T790M transgenic mice were mated to CCSP-rtTA transgenic mice (19) to create double transgenic doxycycline-inducible mice. Mice were given 2 g/kg doxycycline feed (Bio-Serv) starting at 5 weeks of age. Tumor development was monitored by MRI and only mice having tumors confirmed by MRI were included in this study. Nodules were visible by 14–20 weeks post-induction. Mice were housed and cared for at National Cancer Institute-Frederick facilities. NCI-Frederick is accredited by the Association for Assessment and Accreditation of Laboratory Animal Care (AAALAC) International and follows the USPHS Policy for the Care and Use of Laboratory Animals. All the studies were conducted according to an approved Animal Care and Use Committee protocol (20).

Mice were monitored daily for their general health. However, evaluation of survival was terminated 120 days after first NIR-PIT because all mice in control group survived longer than 120 days due to slow growing character similar to human tumor and the oldest mouse age reached close to 1 year old.

Ex vivo fluorescence imaging

To detect the antigen specific distribution of pan-IR700 in the lung tumor, fluorescence imaging was performed. Lungs with tumors were excised from mice 24 hours after injection of 300 μg of pan-IR700. Fluorescence images of IR700 of extracted lung were obtained using a Pearl Imager (LICOR Biosciences, Lincoln, Nebraska, USA) with a 700 nm fluorescence channel.

Fluorescence microscopy

To detect the antigen specific micro-distribution in the lung tumor, fluorescence microscopy was performed. After *ex vivo* fluorescence imaging extracted lung tumors were frozen with OCA compound (SAKURA Finetek Japan Co., Tokyo, Japan) and frozen sections (10 μm thick) were prepared followed by fluorescence microscopy using the BX61 (Olympus America, Inc., Melville, NY, USA) equipped with the following filters; excitation wavelength 590 to 650 nm, emission wavelength 665 to 740 nm long pass for IR700-signal. Transmitted light differential interference contrast (DIC) images were also acquired.

Flow cytometry

For reference, the number of EGFR molecules on A431 cells has already been determined to be 1.5 million per cell (21). A431 cells were purchased from and authenticated by ATCC (Rockville, MD, USA) in 2015 and were not tested in our place. IR700 fluorescence signal from pan-IR700 accumulated on A431 cells is thought to reflect the amount of EGFR on cells. Thus, to estimate the number of EGFR molecules on lung cancer cells, we carried out a flow cytometric analysis. 2×10^5 cells of A431 cells were plated in a 12-chamber culture well and incubated for 24 h. Lung cancer cell suspension was prepared by passing the fragmented lung tumors through 70 μm filters. For both cancer cells medium was replaced with fresh culture medium containing 10 μg/ml of pan-IR700 and incubated for 6 hours at 37 °C. After washing with phosphate buffered saline (PBS), PBS was added. A 488-nm argon ion laser was used for excitation. Signals from cells were collected with a 653- to 669 nm band-pass filter for IR700. Cells were analyzed in a FACS Calibur (BD BioSciences, San Jose, CA, USA). Mean fluorescence intensity (MFI) was quantified using CellQuest software (BD BioScience). The number of EGFR molecules on lung cancer cells was estimated from the ratio $MFI_{lung\ cancer\ cell}$ to MFI_{A431}.

Immunoreactivity of panitumumab-IR700 conjugate

To determine the binding characteristics of panitumumab-IR700, panitumumab was labeled with ^{125}I using the Indo-Gen procedure. The specific activity of the radiolabeled antibody was 17.9 mCi/mg. Cell suspension prepared by passing the fragmented lung tumors through 70 μm filters was resuspended in PBS containing 1 % bovine serum albumin (BSA). ^{125}I-panitumumab (6 ng) was added and incubated for 1 hour on ice. Cells were washed,

pelleted, the supernatant decanted, and counted in a γ-counter (2470 Wizard2, PerkinElmer, Woodland, TX, USA). Nonspecific binding to the cells was examined under conditions of antibody excess by adding 10 μg of nonlabeled panitumumab.

Near infrared photoimmunotherapy

Lung tumor bearing transgenic mice were randomized into 3 groups at least 5 animals for the following treatments: (1) no treatment (control); (2) 150 μg of pan-IR700 i.v. but no NIR light exposure (APC i.v. only); (3)150 μg of pan-IR700 i.v. followed by NIR light at 50 J/cm^2 on day 1 after intravenous injection of pan-IR700 (NIR-PIT). The mice were irradiated with NIR light from 2 directions (each 25 J/cm^2) via the back and front using NIR laser light at 685 to 693 nm wavelength (BWF5-690-8-600-0.37; B&W TEK INC., Newark, DE, USA) (500 $mW/cm^2 \times 50$ s, 25 J/cm^2) while the remainder of the body was shielded from light with aluminum foil. The power density of light in mW/cm^2 was measured with an optical power meter (PM100, Thorlabs, Newton, NJ, USA). These therapies were performed every week for up to 3 weeks. Fluorescence images were not obtained because IR700 fluorescence accumulated within lung tumors was not detectable outside the body.

MRI

Imaging techniques—Under isoflurane anesthesia animals were scanned 1 day before and 3, 6, 13, 20, 27, and 34 days after first NIR-PIT (Figure 1A). MRI was performed on a 3-T scanner using an in-house-built 10 inch saddle shaped mouse receiver coil array (Intera Acieva 3T; Philips Medical Systems, Best, Netherlands). Scout images were obtained to accurately locate the lungs. All mice underwent T2-weighted imaging (T2-WI), T1-weighted spoiled gradient-echo sequence, and balanced-steady-state free precession (b-FFE). The parameters for T2-WI were TR/TE 4000 ms/30 ms, echo train length 6, flip angle (FA) 90, field-of-view (FOV) 80×40 mm, matrix 400×198, pixel size 0.2×0.2 mm, slice thickness and gap 0.6/0 mm, acquisition time 4 min and 32 s, and number of slices 40. The SPGR parameters were TR/TE 16 ms/2.3 ms, FA 30, FOV 70×35 mm, matrix 412×104, pixel size 0.17×0.34 mm, slice thickness and gap 0.3/0 mm, number of excitations 3, acquisition time 1 min and 56 s, and number of slices 60. For b-FFE, the parameters were TR/TE 7.7 ms/2.2 ms, FA 45, FOV 80×41 mm, matrix 472×120, pixel size 0.17×0.34 mm, slice thickness and gap 0.3/0 mm, number of excitations 4, acquisition time 1 min and 38 s, and number of slices 70.

All images were obtained in the coronal plane. Total acquisition time was about 20 min.

Image Analysis—All images were analyzed using Image J software (http://rsb.info.nih.gov/ij/). The volume of each lung tumor was monitored using T2WI beginning with the first MR exam (performed 1 day before first NIR-PIT). The gray level within each tumor region of interest was reduced to a binary image using Otsu's method (22,23). This algorithm assumes that the image contains two classes of pixels following a bi-modal histogram. It then calculates the optimum threshold separating the two classes. We calculated the volume based on pixels above this threshold. Next, the tumor volume ratio was calculated from the tumor volume at each time point divided by the initial volume, 1

day before first NIR-PIT. The five largest lesions were evaluated when multiple lesions were present.

Pathological analysis for treated lung tumor

To evaluate histological changes after NIR-PIT, light microscopy was performed using an Olympus BX61 microscope (Olympus America, Inc., Melville, NY). Lungs with tumors were excised from mice without treatment, 24 hours after injection of pan-IR700 (APC i.v. only) and 24 hours after NIR-PIT (n=3). Extracted lungs with tumors were placed in 10 % formalin and serial 10 μm slice sections were fixed on glass slides with hematoxylin and eosin staining.

Statistical analysis

Statistical analysis was performed with JMP 10 software (SAS Institute, Cary, NC). Steel's test for multiple comparison was used to compare the tumor volume ratio with that of control. The cumulative probability of survival was estimated in each group with a Kaplan-Meier survival curve analysis, and the results were compared with use of the log-rank test. Differences of $p < 0.05$ were considered statistically significant.

RESULTS

Ex vivo fluorescence imaging and fluorescence microscopy

The treatment regimen for *ex vivo* fluorescence imaging and fluorescence microscopy is shown in Figure 2A. On *ex vivo* fluorescence imaging IR700 fluorescence coincided exclusively with lung tumors (Figure 2B). In addition high fluorescence intensity was shown within lung tumors 24 hours after pan-IR700 injection in frozen histologic specimens in the absence of NIR light activation (Figure 2C).

Expression of EGFR and characterization of pan-IR700 in in vitro lung cancer cells

On flow cytometry MFI was 109.1 and 31.0 for A431 cells and lung cancer cells, respectively (Figure 2D). The number of EGFR molecules on A431 cells is known to be approximately 1.5 million per cell (21). Thus, the estimated number of EGFR molecules on lung cancer cells was approximately 0.43 million per cell.

We analyzed the in vitro binding of the pan-IR700 to lung cancer cells in a binding assay using ^{125}I-labeling. After 1 hour incubation, 30.9 % binding was achieved. On the other hand, only 4.6 % binding was observed after the addition of excess panitumumab, suggesting specific binding.

In vivo NIR-PIT

The treatment regimen is shown in Figure 1A. In the control and APC i.v. only group the size of lung tumors increased rapidly with time. On the other hand, in the NIR-PIT group the size of lung tumors increased only gradually with time (Figure 1B). Tumor volume ratio was inhibited significantly in the NIR-PIT group compared with control group ($p < 0.01$ at all time points). No significant difference in tumor volume ratio in the APC i.v. only group compared to the control group was observed ($p = 0.43, 0.34, 0.09, 0.12, 0.19,$ and 0.45 at

day 3, 6, 13, 20, 27, and 34, respectively) (Figure 1C). There was no significant difference in survival among three groups (p = 0.50) (Figure 1D).

Pathological analysis for treated lung tumor

NIR-PIT treated lung tumors showed cellular necrosis and micro-hemorrhage within a background of live but damaged tumor cells. However, no obvious damage was observed in tumors after APC i.v. only and the control group (Figure 3).

DISCUSSION

NIR-PIT has been shown to be effective with a variety of different APCs using subcutaneously xenografted tumors or lung or peritoneal metastatic human tumor models in athymic mice (1–10). However, NIR-PIT has not been tested in spontaneously occurring cancers growing in transgenic mouse models. There is a reason to believe that the spontaneous and heterogeneous nature of these tumors in the context of a wildtype immune response to NIR-PIT could lead to results that differ from xenografts treated with NIR-PIT. Thus, in this study, we evaluated the efficacy of NIR-PIT in spontaneously occurring lung cancers in the hEGFR TL transgenic mouse model.

Our result of *ex vivo* fluorescence imaging and fluorescence microscopy showed that IR700 fluorescence signal was confirmed within the tumor indicating delivery of the antibody-photoabsorber conjugate to the tumor. Moreover, the result of *in vitro* binding of the pan-IR700 to lung cancer cells in a binding assay using ^{125}I-labeling suggested specific binding. Thus, we concluded that the lung cancer in our transgenic mice model expressed EGFR and was able to bind pan-IR700 in a specific manner. Based on flow cytometric analysis the estimated number of EGFR molecules on these lung cancer cells was 0.43 million per cell, about 30 % of EGFR molecules on A431 cells which is a classic EGFR+ cell line used in xenografts (21). These results suggest that lung cancer in this transgenic mouse model had a sufficient number of EGFR molecules, albeit lower than A431, to be an effective target for NIR-PIT with pan-IR700.

Pathological analysis revealed cellular necrosis and micro-hemorrhage within a background of live but damaged tumor cells in NIR-PIT treated lung tumors. In addition change of tumor volume evaluated by MRI showed significant inhibition of tumor growth in NIR-PIT group compared to control groups. Taken together, NIR-PIT was effective for inhibiting lung cancer growth in this transgenic mouse model.

The therapeutic effects of NIR-PIT in this model of lung cancer in a transgenic mouse model seemed to be less effective compared to a comparable study of NIR-PIT in lung metastases from a xenograft model using a 3T3/HER2 cell line expressing human epidermal growth factor receptor type 2 in athymic nude mice (7). This can be explained in a number of ways. First, the transgenic mouse model produced tumors with fewer EGFR molecules compared to A431 cells. Moreover, MRI was used in the transgenic model whereas bioluminescence was used in the xenograft model. MRI can evaluate only morphological change, while luciferase activity can detect early necrotic cell death induced by NIR-PIT preceding the

morphological change (9,16). Thus, in this setting bioluminescence imaging may be more sensitive than MRI to NIR-PIT changes.

Change of tumor volume evaluated by MRI showed significant inhibition of tumor growth in the NIR-PIT group compared to control groups, while there was no significant difference in survival among three groups. New tumors kept developing in our transgenic mouse model as long as mice are fed with doxycycline feed. NIR-PIT would not be effective to new tumors developed during observation because NIR-PIT is effective only to existing tumors when exposing NIR light. Additionally, some newly-developed tumors grew rapidly. Survival could be subjected to overall tumor growth including newly developed, rapidly growing tumors. Thus, although volume of existing tumors were significantly altered by NIR-PIT, no significant difference in survival could be seen.

Another way to overcome the problem of the xenograft tumor model which does not fully represent human cancers is using orthotopic mouse models which can lead to metastasis mimicking to that seen in patients (11,24–28). However, surgical orthotopic implant requires highly trained surgical skills. In addition, tumor microenvironment of implanted tumors might be different from spontaneously arising tumors in transgenic mice or human patients.

A limitation of NIR-PIT is the difficulty in delivering NIR light to the tumor located deep within the body. In mice, NIR light could be delivered into the thoracic cavity using surface illumination, while this is impossible in human patients. In order to deliver NIR light into the human thoracic cavity, direct exposure of NIR light to the thoracic cavity would be necessary using either direct illumination during thoracic surgery or using fibro-optic diffusers via bronchoscopes or thoracoscopes or inserted needles. NIR-PIT combined with surgery to treat residual tumors after surgical resection might be a reasonable way to incorporate NIR-PIT into the management of lung cancer patients.

In conclusion, tumor growth of lung cancer was suppressed after treatment with NIR-PIT in transgenic mice. Serial MRI demonstrated a clear effect on growth rates of tumors without necessary effecting a cure. These results can be readily translated to the human condition, although light will have to be delivered either during surgery, endoscopy or with direct needle placement of fiberoptics. These early results demonstrate promising results in a spontaneously occurring transgenic model adding to the growing list of tumor models that are amenable to NIR-PIT and complementing the growing experience in humans with cancer with NIR-PIT.

Supplementary Material

Refer to Web version on PubMed Central for supplementary material.

Acknowledgments

Abbreviation list

NIR-PIT	near infrared photoimmunotherapy
EGFR	epidermal growth factor receptor
APC	antibody-photo-absorber conjugate
GEM	genetically engineered mouse
MRI	magnetic resonance imaging
hEGFR	human EGFR
TKI	tyrosine kinase inhibitor
mAb	monoclonal antibody
AAALAC	Association for Assessment and Accreditation of Laboratory Animal Care
PBS	phosphate buffered saline
MFI	mean fluorescence intensity
BSA	bovine serum albumin
T2-WI	T2-weighted imaging
b-FFE	balanced-steady-state free precession
FA	flip angle
FOV	field-of-view

References

1. Mitsunaga M, Ogawa M, Kosaka N, Rosenblum LT, Choyke PL, Kobayashi H. Cancer cell-selective in vivo near infrared photoimmunotherapy targeting specific membrane molecules. Nat Med. 2011; 17:1685–91. [PubMed: 22057348]

2. Hanaoka H, Nagaya T, Sato K, Nakamura Y, Watanabe R, Harada T, et al. Glypican-3 targeted human heavy chain antibody as a drug carrier for hepatocellular carcinoma therapy. Mol Pharm. 2015; 12:2151–7. [PubMed: 25955255]

3. Nagaya T, Sato K, Harada T, Nakamura Y, Choyke PL, Kobayashi H. Near Infrared Photoimmunotherapy Targeting EGFR Positive Triple Negative Breast Cancer: Optimizing the Conjugate-Light Regimen. PLoS One. 2015; 10:e0136829. [PubMed: 26313651]

4. Watanabe R, Hanaoka H, Sato K, Nagaya T, Harada T, Mitsunaga M, et al. Photoimmunotherapy targeting prostate-specific membrane antigen: are antibody fragments as effective as antibodies? J Nucl Med. 2015; 56:140–4. [PubMed: 25500827]

5. Nagaya T, Nakamura Y, Sato K, Zhang YF, Ni M, Choyke PL, et al. Near infrared photoimmunotherapy with an anti-mesothelin antibody. Oncotarget. 2016; 7:23361–9. [PubMed: 26981775]

6. Nagaya T, Nakamura Y, Sato K, Harada T, Choyke PL, Kobayashi H. Near infrared photoimmunotherapy of B-cell lymphoma. Mol Oncol. 2016; 10:1404–14. [PubMed: 27511870]

7. Sato K, Nagaya T, Mitsunaga M, Choyke PL, Kobayashi H. Near infrared photoimmunotherapy for lung metastases. Cancer Lett. 2015; 365:112–21. [PubMed: 26021765]

8. Sato K, Choyke PL, Kobayashi H. Photoimmunotherapy of gastric cancer peritoneal carcinomatosis in a mouse model. PLoS One. 2014; 9:e113276. [PubMed: 25401794]

9. Sato K, Hanaoka H, Watanabe R, Nakajima T, Choyke PL, Kobayashi H. Near infrared photoimmunotherapy in the treatment of disseminated peritoneal ovarian cancer. Mol Cancer Ther. 2015; 14:141–50. [PubMed: 25416790]

10. Sato K, Nagaya T, Nakamura Y, Harada T, Choyke PL, Kobayashi H. Near infrared photoimmunotherapy prevents lung cancer metastases in a murine model. Oncotarget. 2015; 6:19474–58.

11. Hoffman RM. Patient-derived orthotopic xenografts: better mimic of metastasis than subcutaneous xenografts. Nat Rev Cancer. 2015; 15:451–2. [PubMed: 26422835]

12. Rygaard J, Povlsen CO. Heterotransplantation of a human malignant tumour to "Nude" mice. Acta Pathol Microbiol Scand. 1969; 77:758–60. [PubMed: 5383844]

13. Garralda E, Paz K, Lopez-Casas PP, Jones S, Katz A, Kann LM, et al. Integrated next-generation sequencing and avatar mouse models for personalized cancer treatment. Clin Cancer Res. 2014; 20:2476–84. [PubMed: 24634382]

14. Rehemtulla A, Stegman LD, Cardozo SJ, Gupta S, Hall DE, Contag CH, et al. Rapid and quantitative assessment of cancer treatment response using in vivo bioluminescence imaging. Neoplasia. 2000; 2:491–5. [PubMed: 11228541]

15. Sato K, Nakajima T, Choyke PL, Kobayashi H. Selective cell elimination in vitro and in vivo from tissues and tumors using antibodies conjugated with a near infrared phthalocyanine. RSC Adv. 2015; 5:25105–14. [PubMed: 25866624]

16. Mitsunaga M, Nakajima T, Sano K, Kramer-Marek G, Choyke PL, Kobayashi H. Immediate in vivo target-specific cancer cell death after near infrared photoimmunotherapy. BMC Cancer. 2012; 12:345. [PubMed: 22873679]

17. Sato K, Watanabe R, Hanaoka H, Harada T, Nakajima T, Kim I, et al. Photoimmunotherapy: comparative effectiveness of two monoclonal antibodies targeting the epidermal growth factor receptor. Mol Oncol. 2014; 8:620–32. [PubMed: 24508062]

18. Sano K, Nakajima T, Choyke PL, Kobayashi H. Markedly enhanced permeability and retention effects induced by photo-immunotherapy of tumors. ACS Nano. 2013; 7:717–24. [PubMed: 23214407]

19. Tichelaar JW, Lu W, Whitsett JA. Conditional expression of fibroblast growth factor-7 in the developing and mature lung. J Biol Chem. 2000; 275:11858–64. [PubMed: 10766812]

20. Guide for the Care and Use of Laboratory Animals. Washington, DC: National Academy Press; 1996.

21. Barrett T, Koyama Y, Hama Y, Ravizzini G, Shin IS, Jang BS, et al. In vivo diagnosis of epidermal growth factor receptor expression using molecular imaging with a cocktail of optically labeled monoclonal antibodies. Clin Cancer Res. 2007; 13:6639–48. [PubMed: 17982120]

22. Sezgin M, Sankur B. Survey over image thresholding techniques and quantitative performance evaluation. J Electron Imaging. 2004; 13:146–68.

23. Otsu N. A threshold selection method from gray-level histograms. IEEE Trans Sys Man Cyber. 1979; 9:62–6.

24. Astoul P, Colt HG, Wang X, Boutin C, Hoffman RM. "Patient-like" nude mouse metastatic model of advanced human pleural cancer. J Cell Biochem. 1994; 56:9–15. [PubMed: 7806595]

25. Wang X, Fu X, Hoffman RM. A new patient-like metastatic model of human lung cancer constructed orthotopically with intact tissue via thoracotomy in immunodeficient mice. Int J Cancer. 1992; 51:992–5. [PubMed: 1639545]

26. Yang M, Hasegawa S, Jiang P, Wang X, Tan Y, Chishima T, et al. Widespread skeletal metastatic potential of human lung cancer revealed by green fluorescent protein expression. Cancer Res. 1998; 58:4217–21. [PubMed: 9766640]

27. Yano S, Zhang Y, Miwa S, Kishimoto H, Urata Y, Bouvet M, et al. Precise navigation surgery of tumours in the lung in mouse models enabled by in situ fluorescence labelling with a killer-reporter adenovirus. BMJ Open Respir Res. 2015; 2:e000096.

28. Zhang Y, Zhang N, Zhao M, Hoffman RM. Real-time Non-invasive Spectral Imaging of Orthotopic Red Fluorescent Protein-expressing Lung Tumor Growth in Nude Mice. Anticancer Res. 2015; 35:3755–9. [PubMed: 26124318]
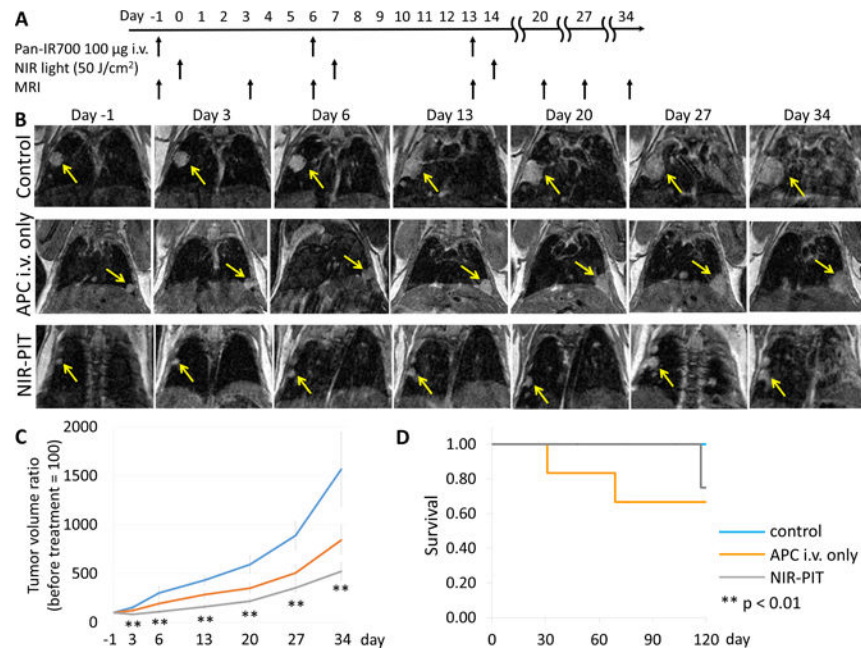
Figure 1.

In vivo effect of NIR-PIT on lung tumor. (A) NIR-PIT regimen of APC administration and NIR light exposure is shown (n = 6, 6, and 8 mice in control, APC i.v. and NIR-PIT group, respectively). MR images were obtained at each time point as indicated. (B) MR imaging of lung tumor bearing mice. In control and APC i.v. only animals the size of the lung tumor increased rapidly, while in the NIR-PIT group of the lung tumors increased only gradually demonstrating an effect on tumor growth rates. (C) Tumor volume ratio was inhibited significantly in the NIR-PIT group compared with control group (p < 0.01 at all time points), while no significant difference in tumor volume ratio in APC i.v. only group compared to control group was observed. (D) There was no significant difference in survival among three groups (p = 0.50).
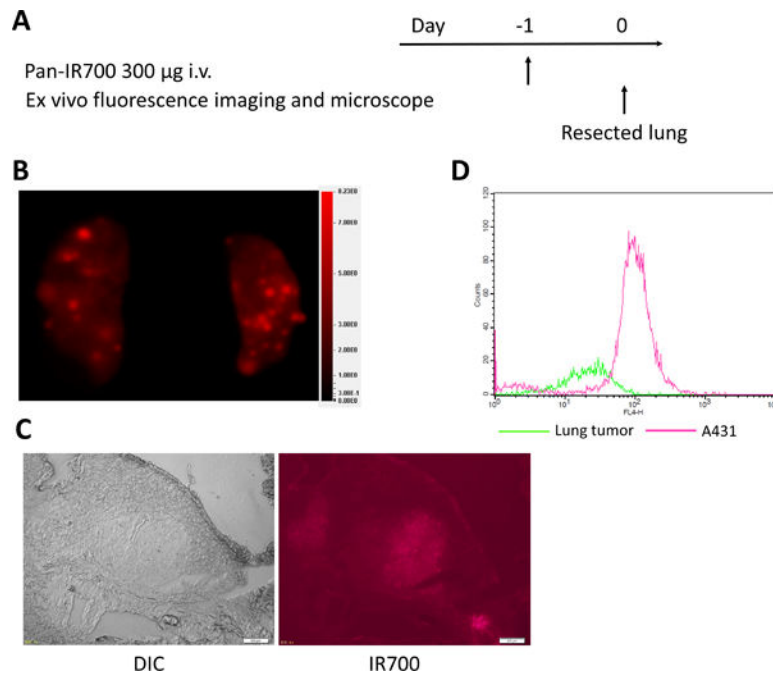
Figure 2.
Ex vivo fluorescence imaging and histological fluorescence distribution of lung tumor. (A) The regimen for *ex vivo* imaging is shown. (B) IR700 fluorescence image of extracted lungs. Lung tumors show high fluorescence signal. (C) Differential interference contrast (DIC) and fluorescence microscopy images of lung tumors. High fluorescence intensity is shown in a lung tumor 24 hours after injection of pan-IR700. Scale bars = 200 μm. (D) Flow cytometric analysis. Mean fluorescence intensity was 109.1 and 31.0 for A431 cells and lung cancer cells, respectively.
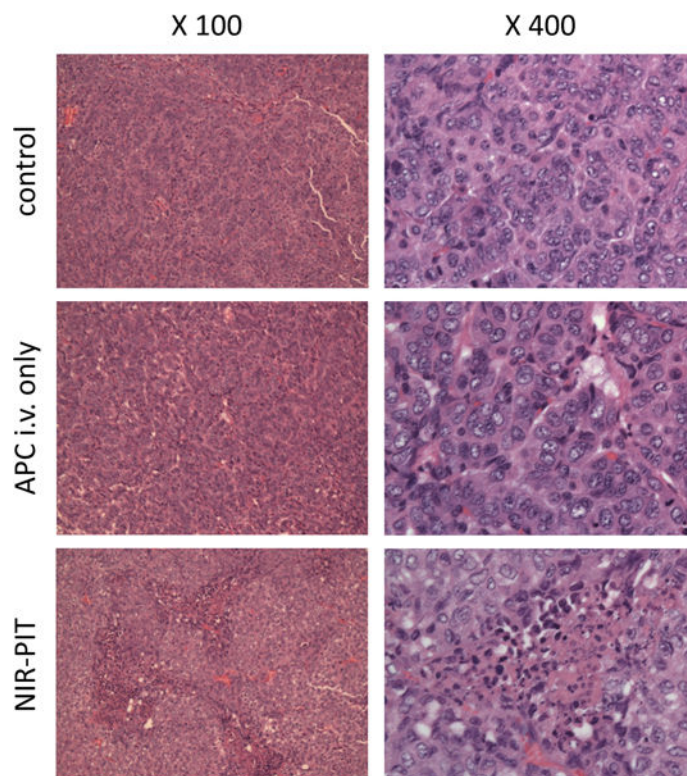
Figure 3.
Resected lung tumors stained with hematoxylin and eosin are shown. Tumors in control and APC only groups contain healthy, typical adenocarcinoma cells with dark nuclei and eosinophilic cytoplasm in ×400 images. A tumor after NIR-PIT therapy contains large numbers of necrotic cells that are shown typically less dark nuclei and eosinophilic cytoplasm with some vacuolar degeneration than healthy cancer cells with micro-hemorrhage and infiltration of inflammatory mononuclear cells in the ×400 image. These damaged cancer cells were widely seen in light red color in the ×100 image (left panel) of a tumor after NIR-PIT, while no such damaged cell was observed in both ×100 and ×400 images of APC i.v. alone without NIR light as well as no treatment control. These histopathological changes were consistent in all tumors examined in each group.